Supporting Information

$Ti_3C_2T_x$ MXene embedded metal-organic framework-based porous electrospun carbon nanofibers as a freestanding electrode for supercapacitors

Ishwor Pathak[a,b], Debendra Acharya[a], Kisan Chhetri[a], Prakash Chandra Lohani[a,b], Subhangi Subedi[c], Alagan Muthurasu[a], Taewoo Kim[a], Tae Hoon Ko[a], Bipeen Dahal[a,d]*, Hak Yong Kim[a,e] *

[a] Department of Nano Convergence Engineering, Jeonbuk National University, Jeonju, 54896, Republic of Korea

[b] Department of Chemistry, Amrit Campus, Tribhuvan University, Kathmandu 44613, Nepal

[c] Department of Chemistry, Tri-Chandra Multiple Campus, Tribhuvan University, Kathmandu 44613, Nepal

[d] Central Department of Chemistry, Tribhuvan University, Kathmandu 44613, Nepal

[e] Department of Organic Materials and Fiber Engineering, Jeonnbuk National University, Jeonju 561-756, Republic of Korea

Corresponding Author's Email: khy@jbnu.ac.kr / dahalbipeen@jbnu.ac.kr

Materials

Titanium aluminum carbide MAX phase (≥90%, ≤40 μm particle size) and lithium fluoride (<100 μm, ≥99.98% trace metal basis) were obtained from Sigma–Aldrich Co., St. Louis, MO, USA. Cobalt nitrate hexahydrate (97.0%), 2-methylimidazole (99.0%), methanol (99.5%), dimethylformamide (DMF, 99.5%%), hydrochloric acid (35.0%), nitric acid (60.0%) and polyacrylonitrile (PAN, MW = 150,000) were provided by Samchun Co. Ltd., Seoul, Korea. All chemicals were of analytical grade and used without further purification.

Preparation of Co_3O_4@NF

Cobalt oxide nanohairs over nanosheets on nickel foam (NF) were prepared by following the protocol of our previous work with slight modifications.[1,2] Briefly, a piece of NF (3×3 cm^2) was dipped in 2 M HCl (25 mL) and sonicated for 15 minutes. Then, NF was again sonicated for 5 minutes with DI water, washed with acetone, and dried in an oven for 6 h. Cobalt nitrate hexahydrate (1.164 g), urea (1.2 g), and ammonium fluoride (0.28 g) were dissolved in DI water (110 mL) and stirred for 30 minutes to make the solution homogenous. The solution was then

transferred to a 150-mL Teflon vessel. Then, a piece of washed and dried NF was dipped in the solution and autoclaved for 6 h at 120 °C. After cooling to room temperature, the NF and powder were collected, washed with DI water and ethanol and dried in an oven at 60 °C for 12 h. Furthermore, the nanostructure of the NF was annealed at 350 °C for 30 minutes in an air atmosphere for the conversion of cobalt hydroxide to cobalt oxide.

Structure and morphology characterizations

The structure and morphology of MXene, MX-5@PCNF, and other control samples were characterized by field emission scanning electron microscopy (FESEM; JEOL, JSM-6701F, Tokyo, Japan) equipped with an energy-dispersive X-ray spectrometer (EDX). Transmission electron microscopy (TEM: JEOL, JEM-2010, Tokyo, Japan), high-resolution TEM (HR-TEM), and selected area electron diffraction (SAED) were performed at 200 kV for microstructural analysis. The height profile of the individual MXene nanosheets was measured by atomic force microscopy (AFM, Bruker, Multimode-8, Billerica, MA, USA) under ambient laboratory conditions. Phase structural analysis of the samples was studied by X-ray diffraction (XRD, Rigaku Corporation, Tokyo, Japan, Cu Kα radiation, λ=1.5406 Å). A Raman study was carried out to study the defects and graphitization in the samples (RES-100S, Bruker, helium-neon laser, λ = 532.06 nm). The surface chemistry of the samples was examined by performing X-ray photoelectron spectrometry (Nexsa XPS system, ThermoFisher Scientific, Horsham, UK). The obtained high-resolution XPS spectra were deconvoluted by Casa-XPS software to determine the chemical bonding state. The nitrogen adsorption-desorption experiment was performed by an adsorption analyzer (Micromeritics, 3Flex Version 5.00, Norcross, GA, USA) to determine the Brunauer-Emmett-Teller (BET) specific area, total pore volume, and pore size distribution. Thermogravimetric analysis (TGA) (Universal V4 5A TA instrument, SDT Q600) of samples was performed in a nitrogen atmosphere from room temperature to 1000 °C at a heating rate of 10 °C min^{-1}.

Electrochemical measurements

The electrochemical tests were performed in a VersaSTAT-4 electrochemical workstation (AMETEK, Inc., Berwyn, PA, USA) at room temperature using a 3 M aqueous KOH electrolyte solution. The prepared materials were directly used as freestanding electrodes without any binders or additives. In a three-electrode system, the prepared freestanding electrode material MX-5@PCNF (1×1 cm^2, 0.002 g) and other control samples were used for the working electrode (WE),

Ag/AgCl was used as the reference electrode, and platinum was used as the counter electrode. Cyclic voltammetry (CV), galvanostatic charge-discharge (GCD), and electrochemical impedance spectroscopy (EIS) measurements were performed to measure the capacitive behaviors and specific capacitance of the electrode materials. EIS was performed from the frequency range of 10^5 to 10^{-2} Hz at a 5 mV amplitude, and the obtained data were fitted with ZSwimpWin software. The specific capacitance (C_s) of the prepared electrodes and the assembled symmetric supercapacitor (SSC) and asymmetric supercapacitor (ASC) devices were calculated from their respective galvanostatic charge-discharge (GCD) curves by using Equation S1.

$$C_s = \frac{I_d \times \Delta t}{\Delta V \times m} \qquad (S1)$$

where I_d, Δt, m, and ΔV are the discharge current (A), discharge time (s), mass of active material (g), and working potential range (V), respectively.

Fabrication of symmetric and asymmetric supercapacitor devices

Aqueous 3 M KOH was used as an electrolyte in both SSC and ASC devices. Two pieces of optimized freestanding MX-5@PCNF having the same weight (0.005g each) and a separator (KOH soaked cellulose based filter paper) were directly used for the fabrication of the SSC device in a sandwich configuration. For ASC device fabrication, MX-5@PCNF coated over nickel foam was used as a negative electrode. For this electrode, a slurry of MX-5@PCNF, polymer binder, and conductive additive at a mass ratio of 8:1:1 was prepared and coated over nickel foam. The most commonly studied/used Co_3O_4@NF was used as a positive electrode. The optimal mass ratio of positive to negative electrodes for the ASC device was calculated according to Equation S2.

$$\frac{m_+}{m_-} = \frac{C_- \times V_-}{C_+ \times V_+} \qquad (S2)$$

where m_+, m_-, C_+, C_-, V_+, and V_- are the mass (g), specific capacitance (F g^{-1}), and potential window (V) of the positive and negative electrodes, respectively.

Mass balancing calculation

$C_+ = 1891$ F g^{-1}

$C_- = 572.7$ F g^{-1}

$V_+ = 0.45$ V

$V_- = 1.0$ V

Therefore, $m_+/m_- = 1:1.48$

Mass of MX-5@PCNF (1 cm^2) = 0.0052g

Mass of active material (Co_3O_4) on positive electrode = 0.0035g

The energy density (E) in Wh kg^{-1} and power density (P) in W kg^{-1} of the symmetric and asymmetric devices were calculated according to Equations S3 and S4, respectively.

$$E = \frac{1}{2\times 3.6} CV^2 \qquad (S3)$$

$$P = \frac{E \times 3600}{t_d} \qquad (S4)$$

where C is the specific capacitance (F g^{-1}), t_d is the discharge time in seconds (s), and V is the voltage of the device.

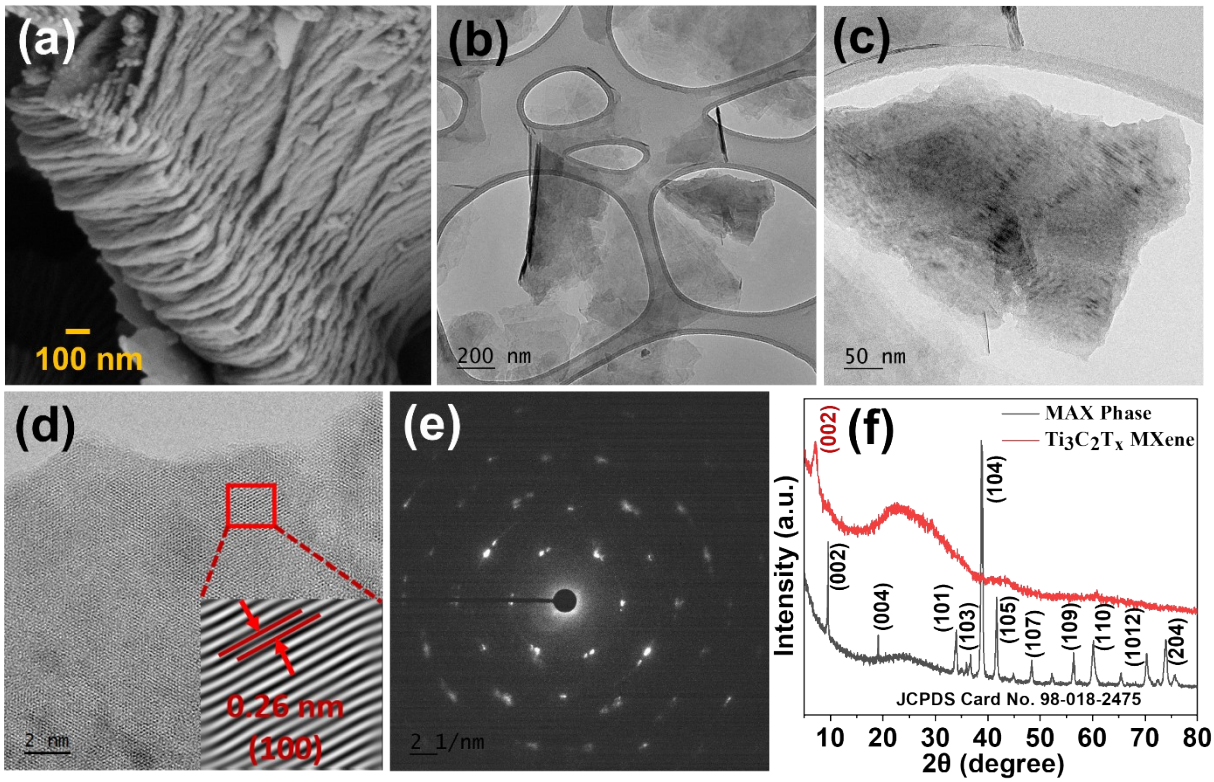

Fig. S1. (a) FESEM image of freeze-dried etched $Ti_3C_2T_x$ MXene, (b) and (c) TEM images of delaminated MXene nanosheets, (d) HR-TEM image, (e) SAED patterns, and (f) XRD patterns of Ti_3AlC_2 MAX phase and $Ti_3C_2T_x$ MXene.

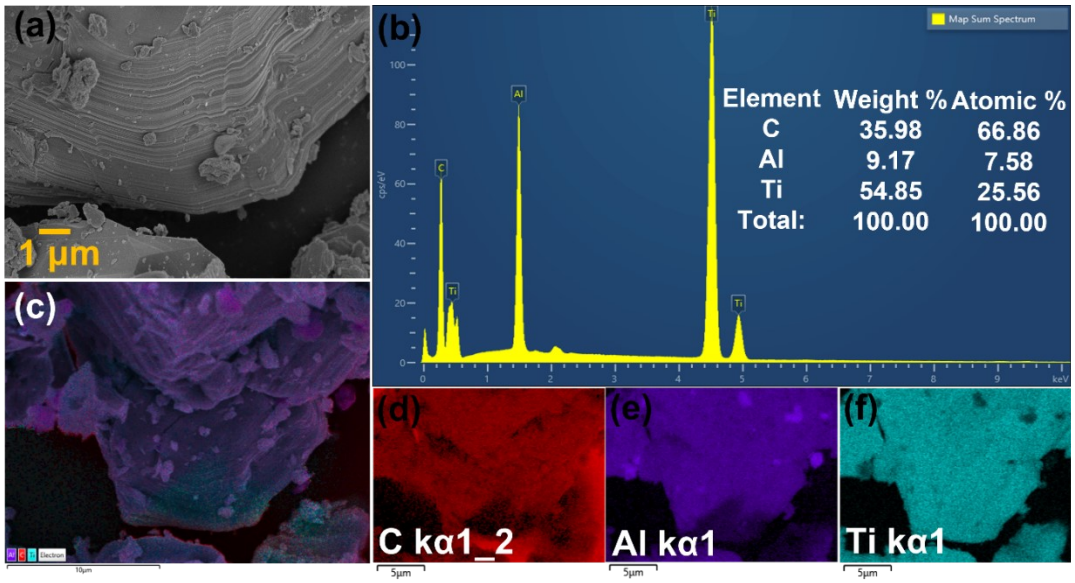

Fig. S2. (a) FESEM image of Ti_3AlC_2 MAX phase. (b) EDX spectrum of Ti_3AlC_2 MAX phase (inset: weight and atomic percentage of the different elements), (c) sum elemental mapping spectrum, and elemental mapping spectra of (d) C, (e) Al, and (f) Ti.

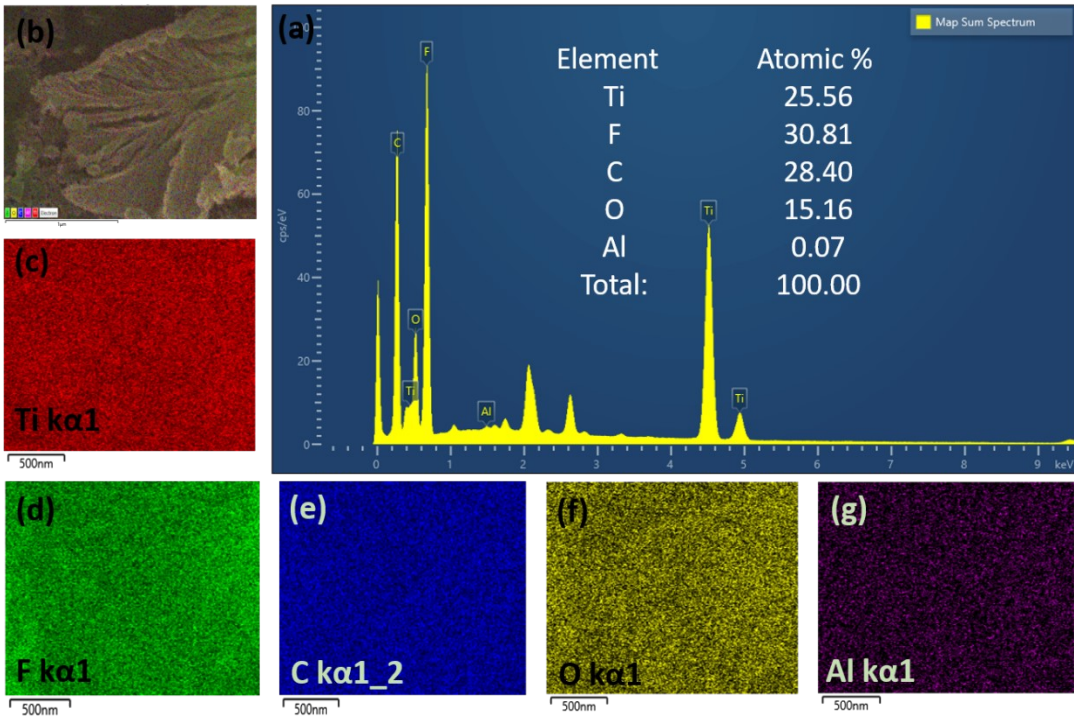

Fig. S3. EDX analysis of $Ti_3C_2T_x$ MXene nanosheet, (a) EDX spectrum (inset: atomic percentage of the different elements), (b) sum elemental mapping spectrum, and elemental mapping spectra of (c) Ti, (d) F, (e) C, (f) O, and (g) Al.

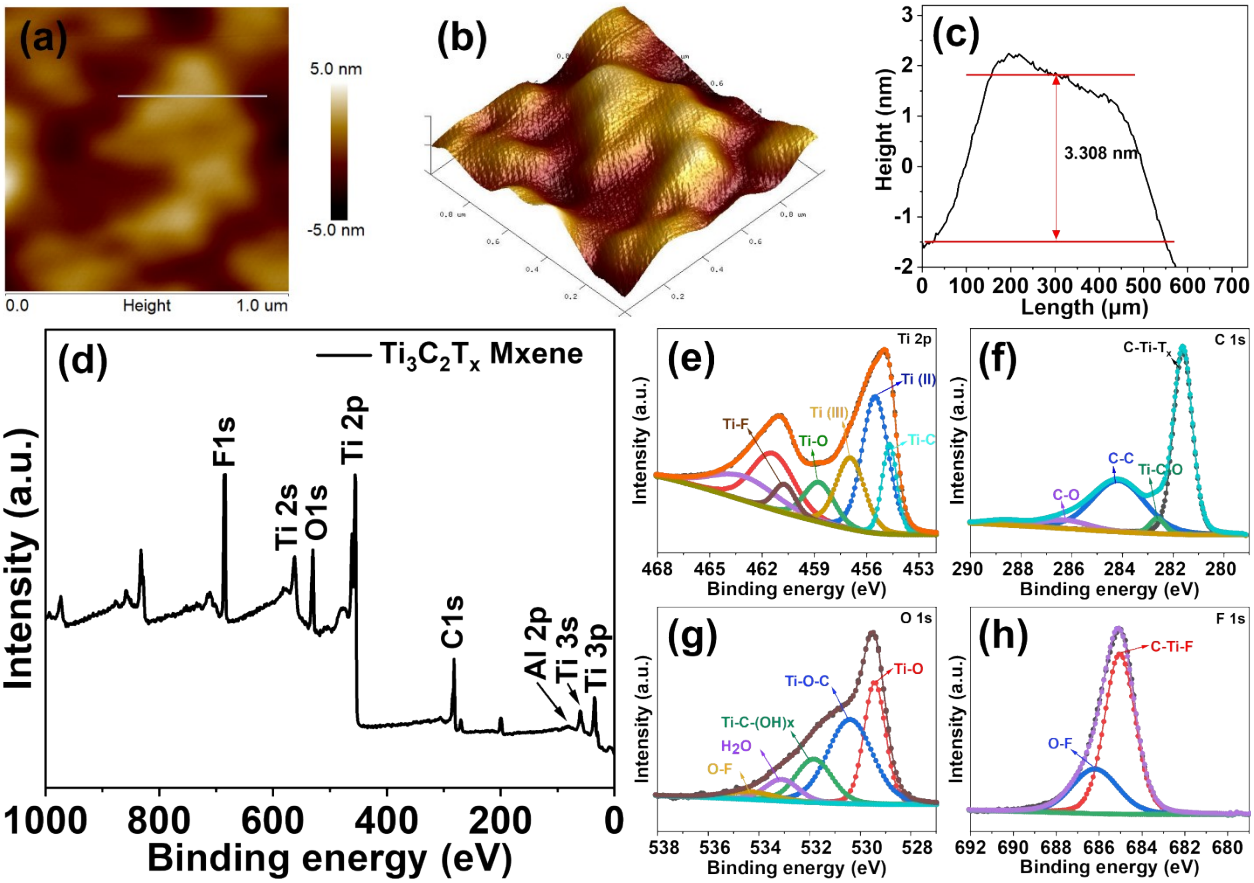

Fig. S4. (a-c) AFM analysis of MXene nanosheet, (a) 2D image, (b) 3D image, and (c) relevant height profile, (d) XPS survey spectra of $Ti_3C_2T_x$ MXene, and high resolution XPS spectrum of MXene deconvoluted for (e) Ti 2p, (f) C 1s, (g) O 1s, and (h) F 1s.

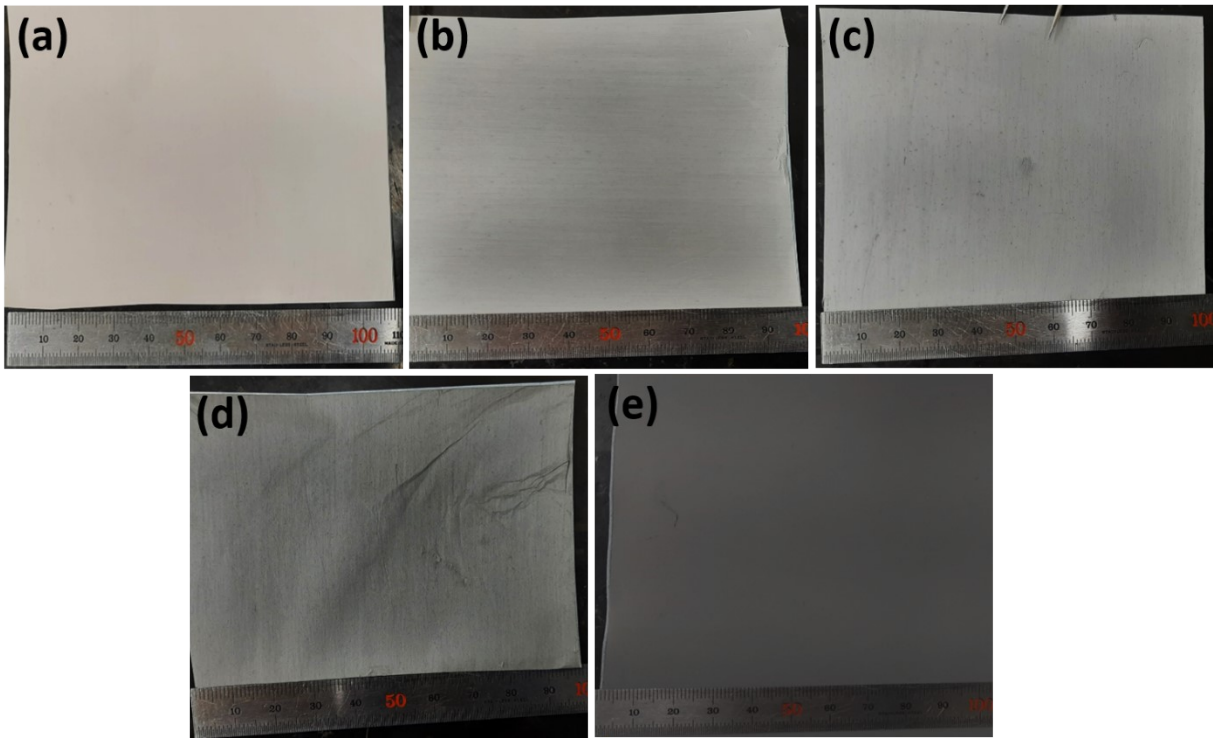

Fig. S5. Digital images of electrospun fiber containing cobalt salt and different wt % of MXene: (a) 0% MXene, (b) 1% MXene, (c) 2% MXene, (d) 5% MXene, and (e) 10% MXene.

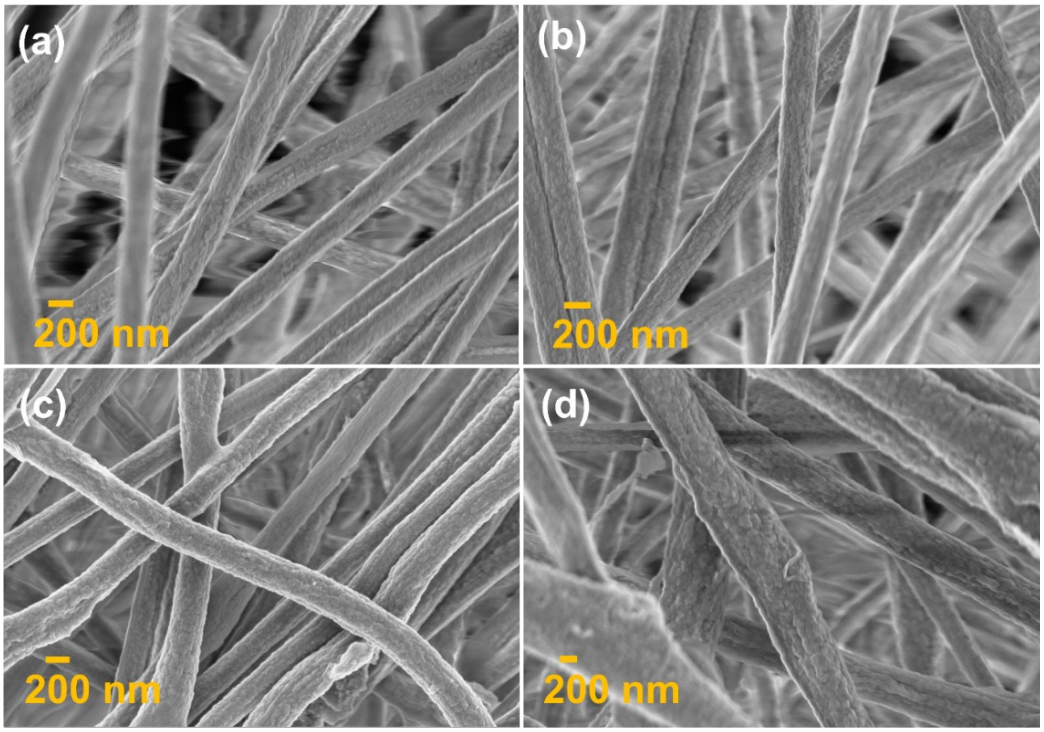

Fig. S6. FESEM images of electrospun mats containing different wt % of MXene. (a) MX-1/$(Co_3)_2$@PAN, (b) MX-2/$(Co_3)_2$@PAN, (c) MX-5/$(Co_3)_2$@PAN, and (d) MX-10/$(Co_3)_2$@PAN.

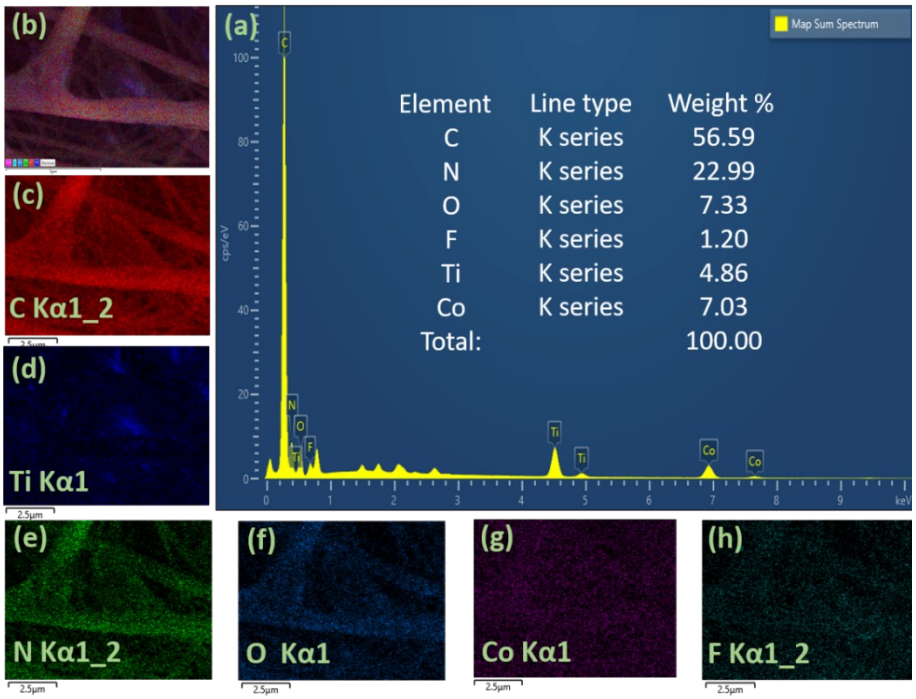

Fig. S7. EDX analysis of MX-5/$Co(No_3)_2$@PAN fiber: (a) EDX spectrum (inset: line type and wt % of the different elements), (b) sum elemental mapping spectrum, and elemental mapping spectra of (c) C, (d) Ti, (e) N, (f) O, (g) Co, and (h) F.

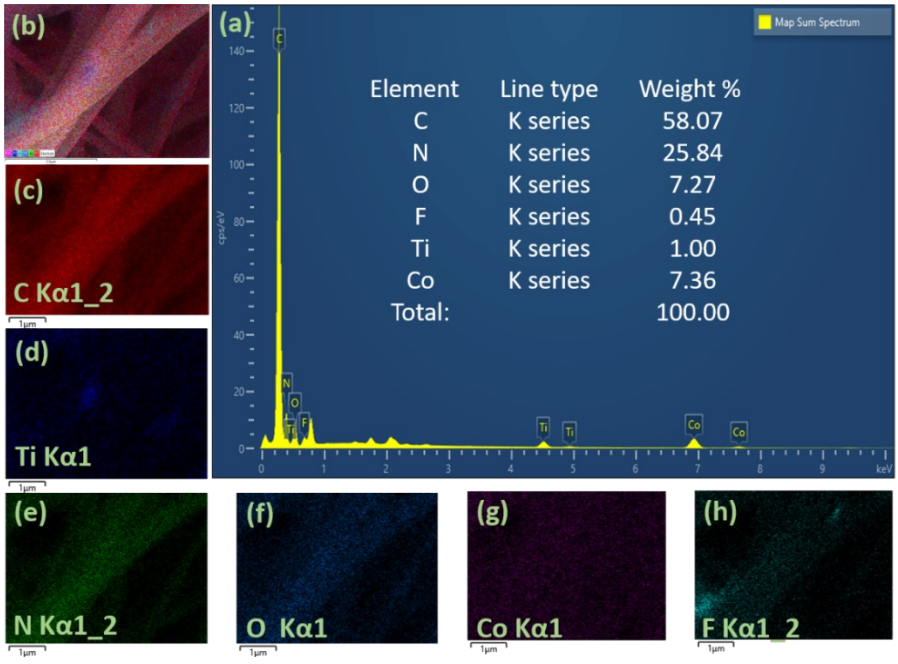

Fig. S8. EDX analysis of MX-1/$Co(No_3)_2$@PAN fiber: (a) EDX spectrum (inset: line type and wt % of the different elements), (b) sum elemental mapping spectrum, and elemental mapping spectra of (c) C, (d) Ti, (e) N, (f) O, (g) Co, and (h) F.

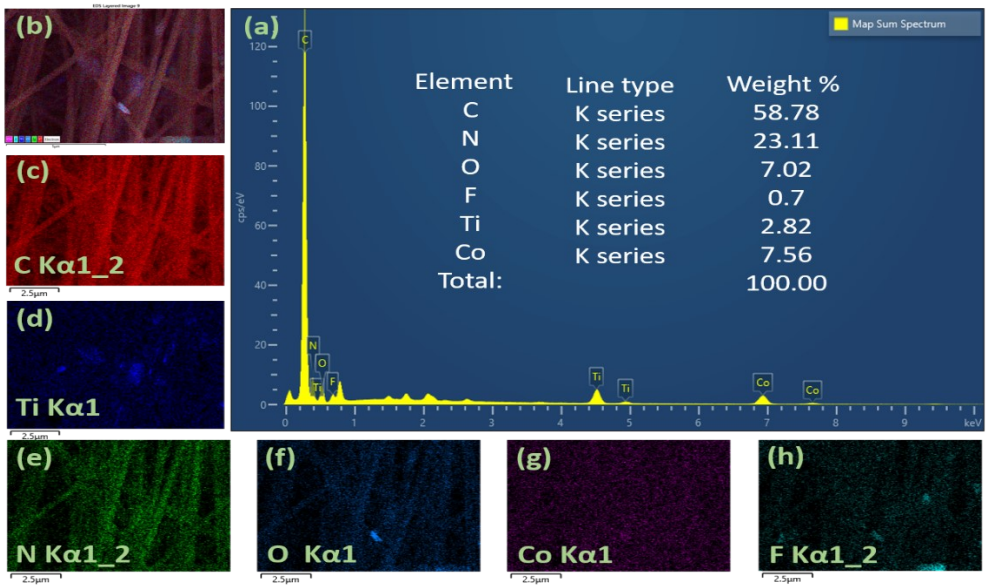

Fig. S9. EDX analysis of MX-2/$Co(No_3)_2$@PAN fiber: (a) EDX spectrum (inset: line type and wt % of the different elements), (b) sum elemental mapping spectrum, and elemental mapping spectra of (c) C, (d) Ti, (e) N, (f) O, (g) Co, and (h) F.

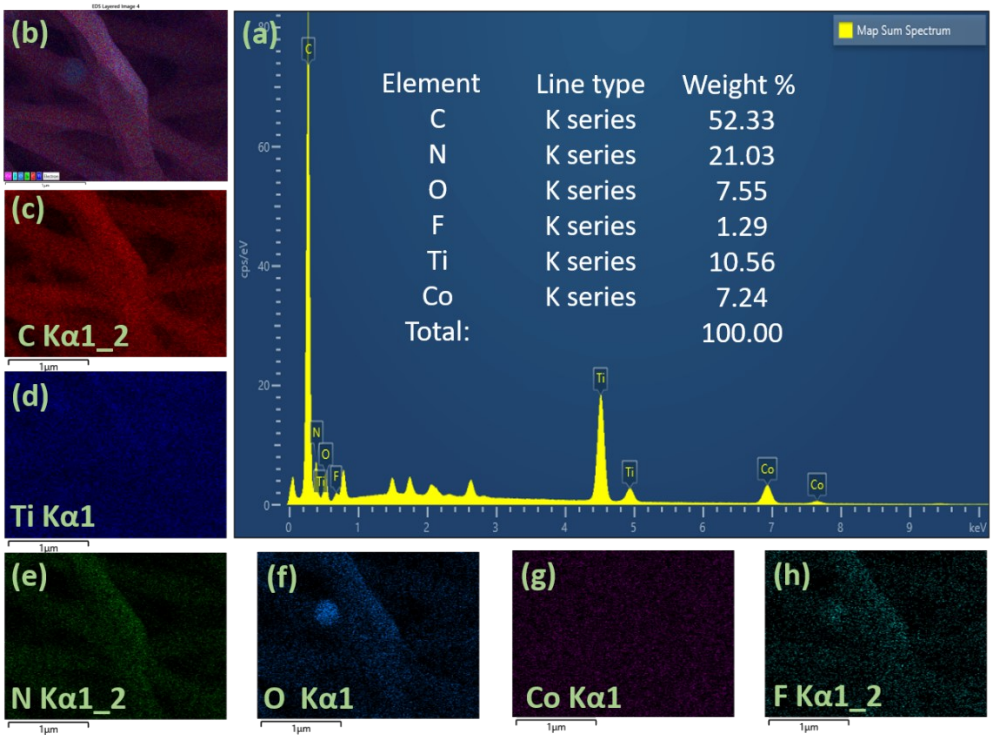

Fig. S10. EDX analysis of MX-10/$Co(No_3)_2$@PAN fiber: (a) EDX spectrum (inset: line type and wt % of the different elements), (b) sum elemental mapping spectrum, and elemental mapping spectra of (c) C, (d) Ti, (e) N, (f) O, (g) Co, and (h) F.

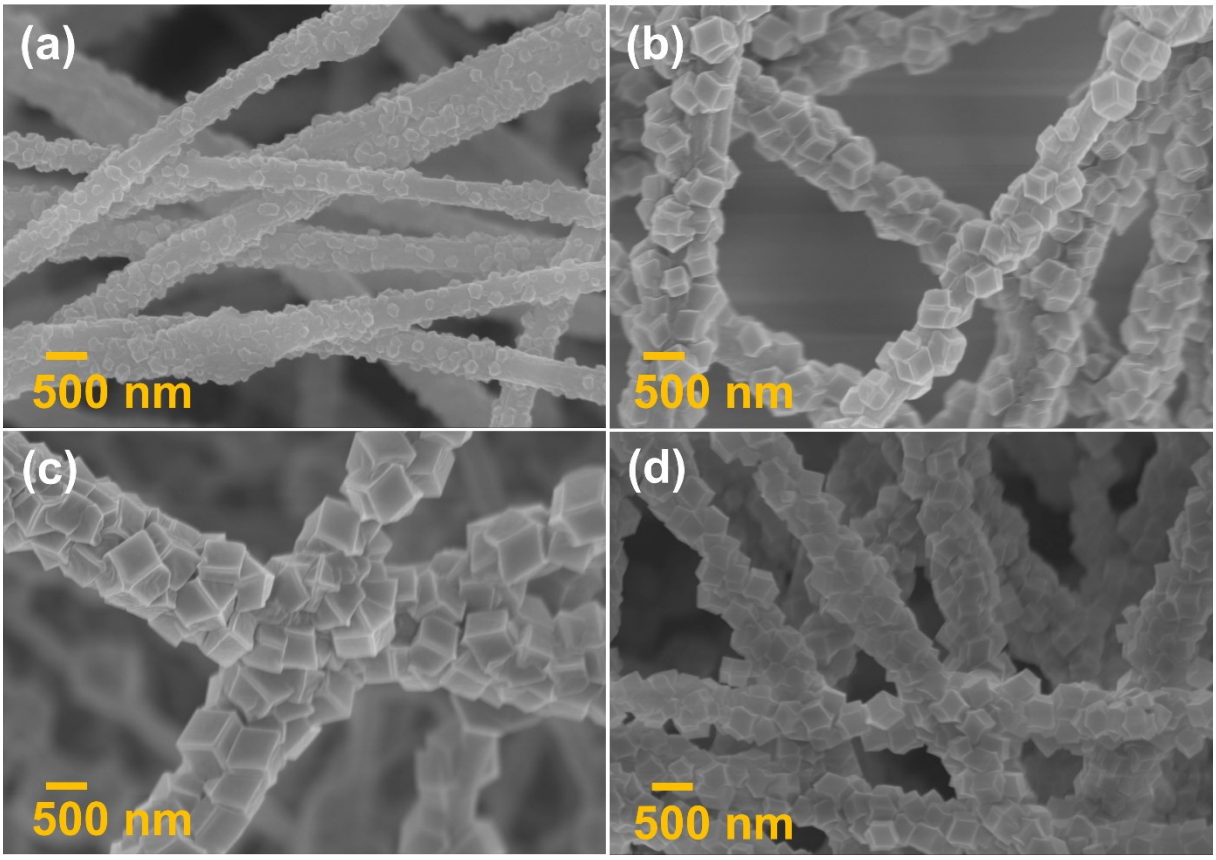

Fig. S11. FESEM images of MX-5/ZIF67@PAN prepared at different aging times. (a) 2 h, (b) 8 h, (c) 16 h, and (d) 24 h.

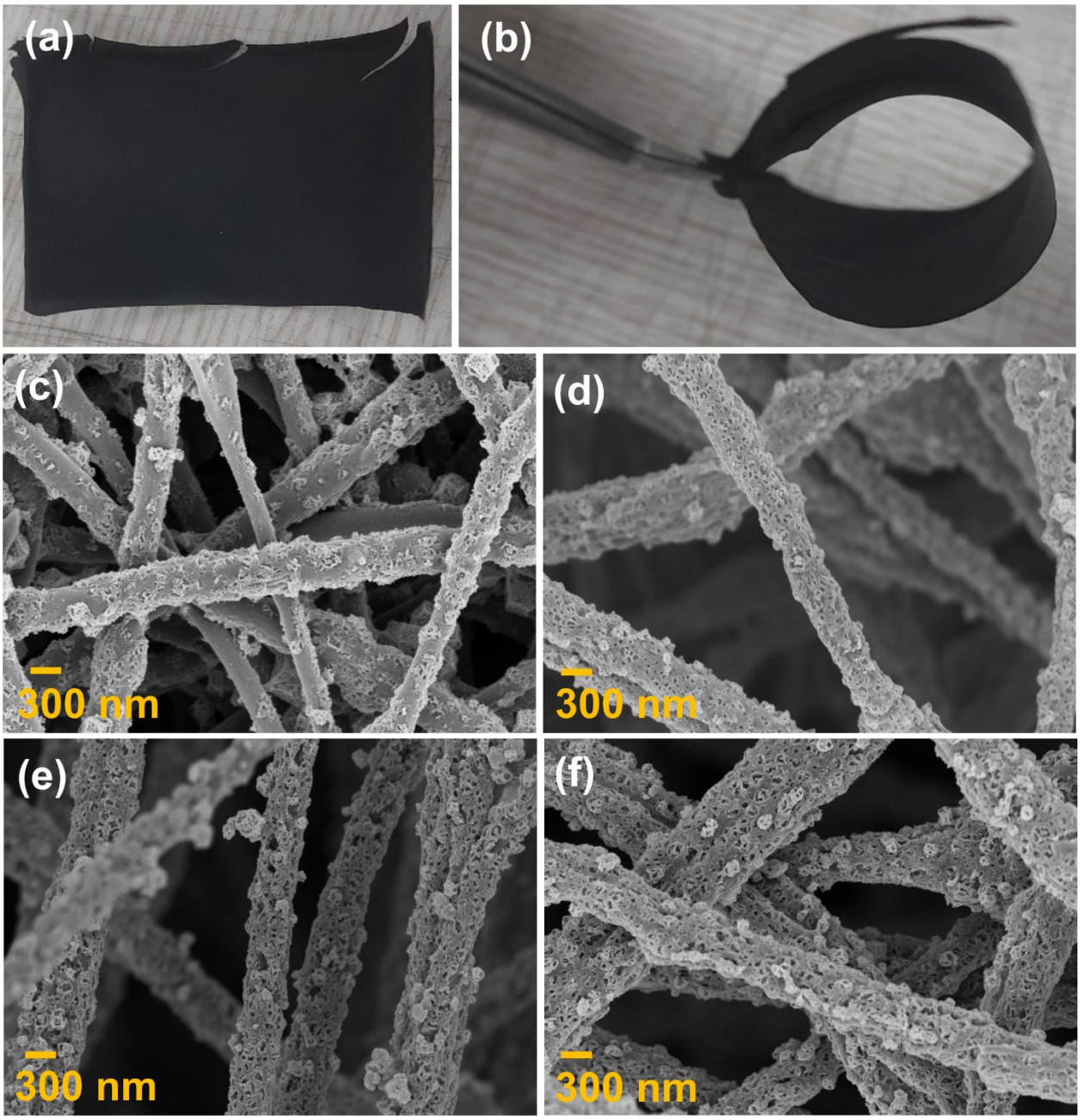

Fig. S12. (a,b) Digital images of black flexible MX-5@PCNF mat, and representative FESEM images of (c) PCNF, (d) MX-1@PCNF, (e) MX-2@PCNF, and (f) MX-10@PCNF.

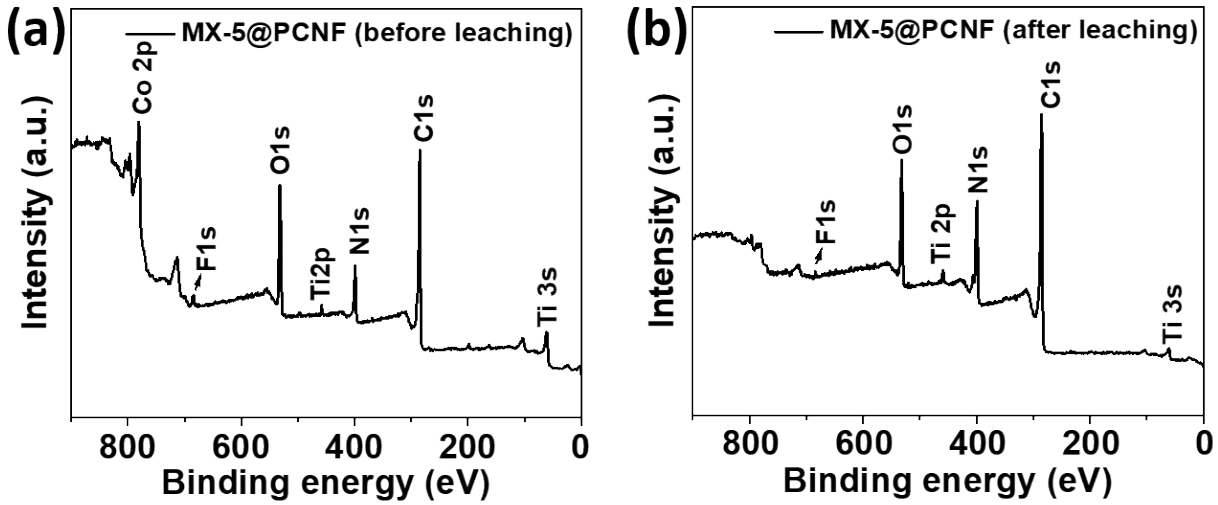

Fig. S13. Low-resolution XPS spectra of MX-5@PCNF before and after acid leaching.

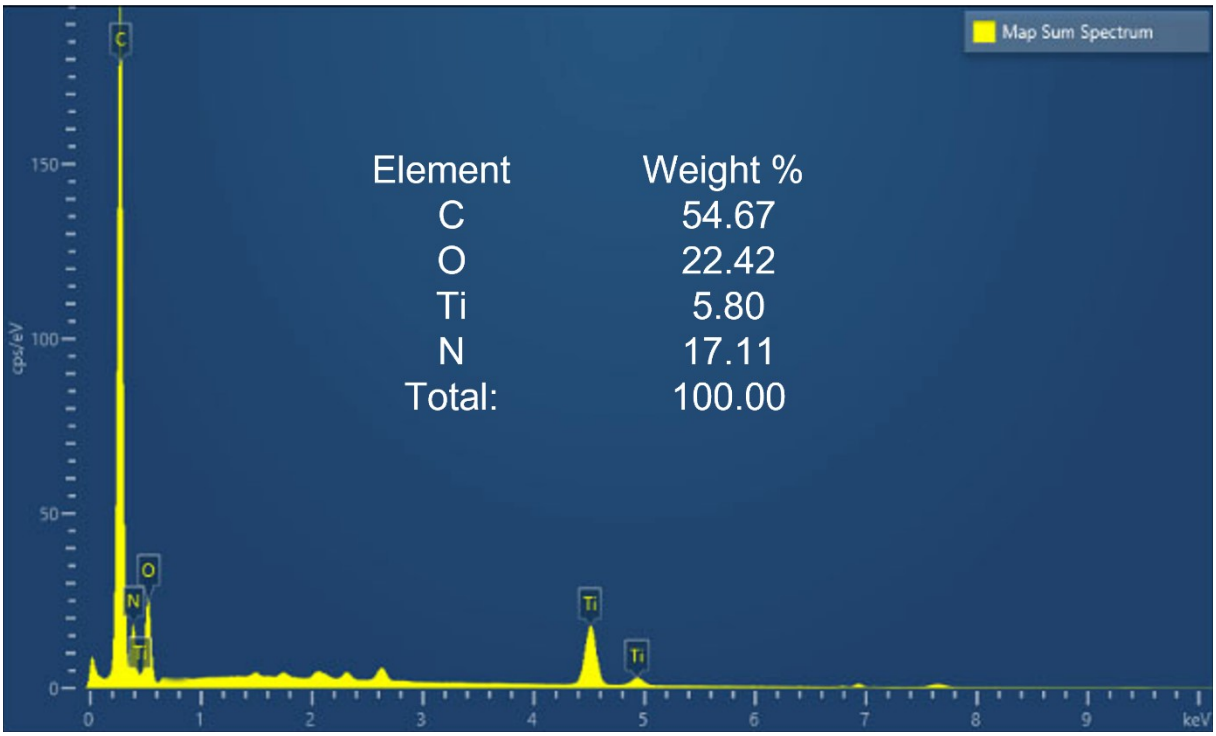

Fig. S14. EDX spectrum from HRTEM image of MX-5@PCNF (inset: weight percentage of different elements).

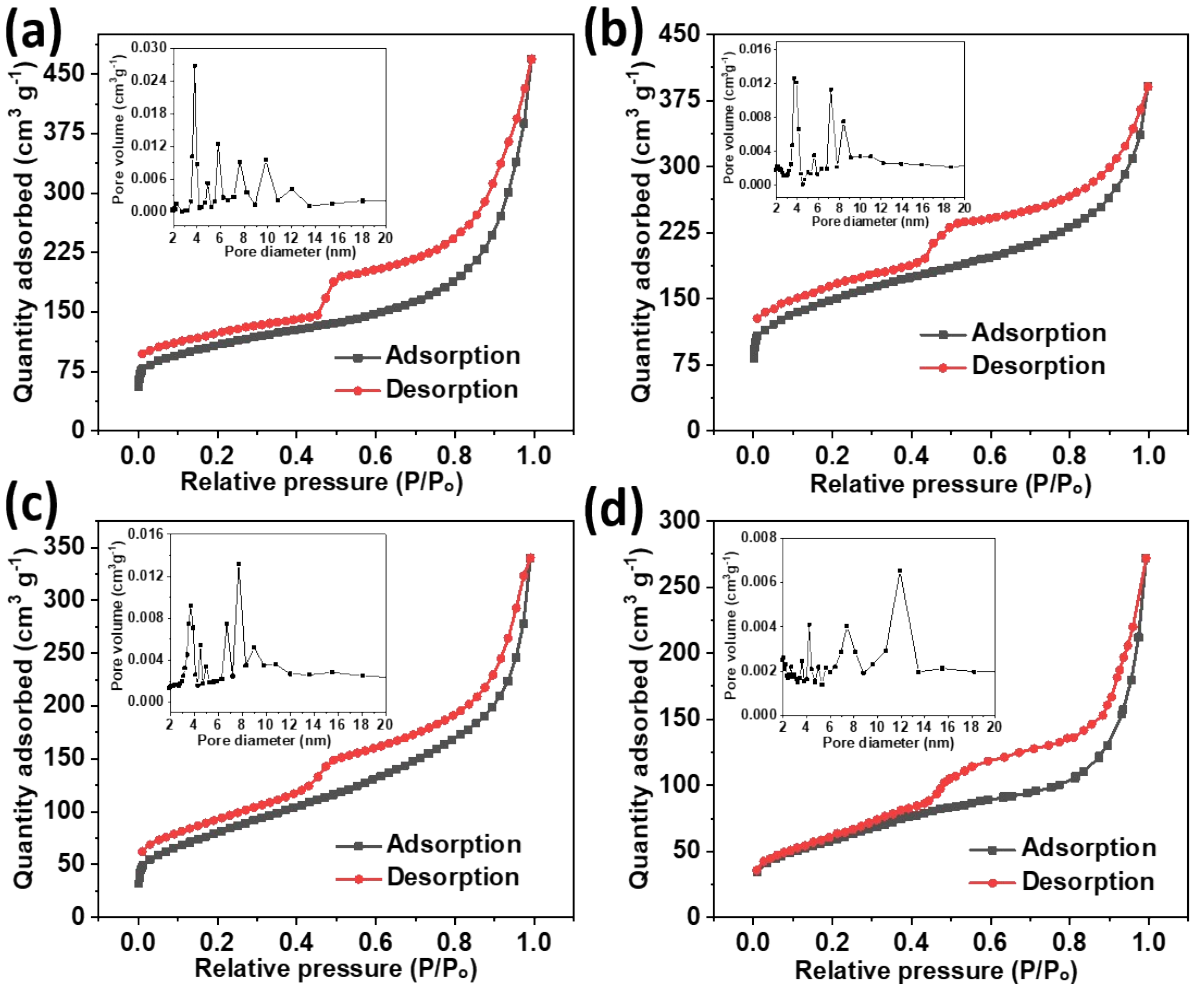

Fig. S15. Adsorption isotherms and pore size distribution (inset) of (a) MX-10@PCNF, (b) MX-2@PCNF, (c) MX-1@PCNF, and (d) PCNF.

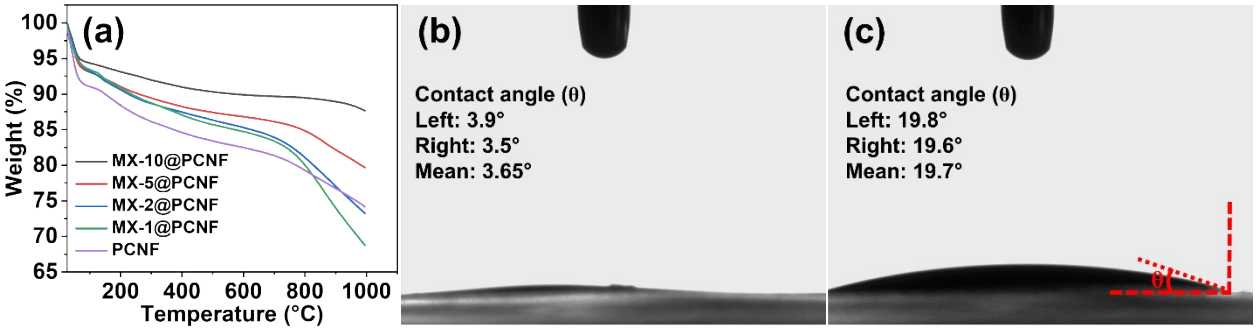

Fig. S16. (a)TGA curves of different samples, and photographs of aqueous droplets attached on the surface of (b) MX-5@PCNF, and (c) PCNF with their respective contact angles.

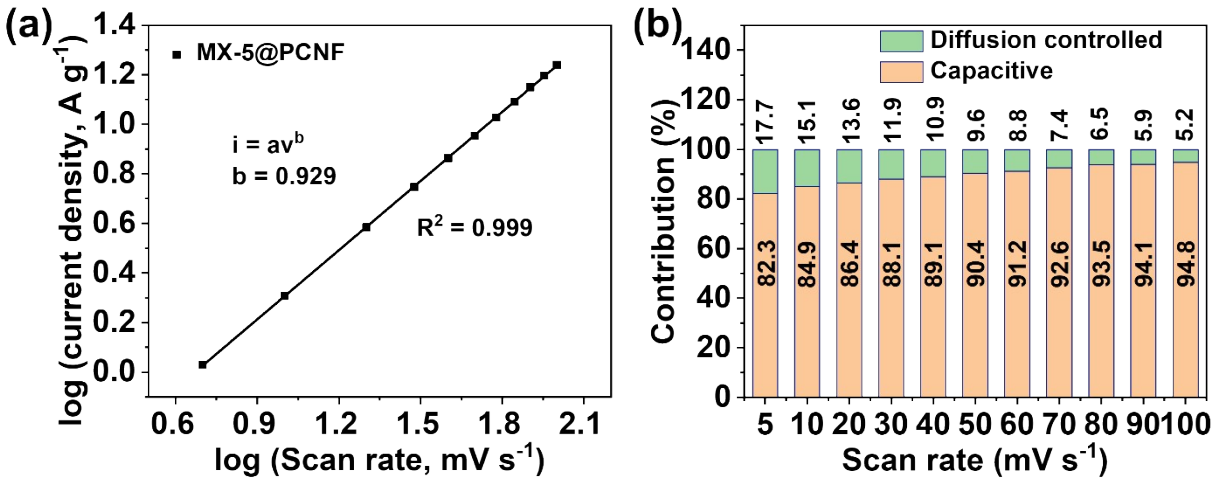

Fig. S17. (a) The plot of log (scan rate) vs log (current density) for MX-5@PCNF, and (b) percentage contribution plot at different scan rates.

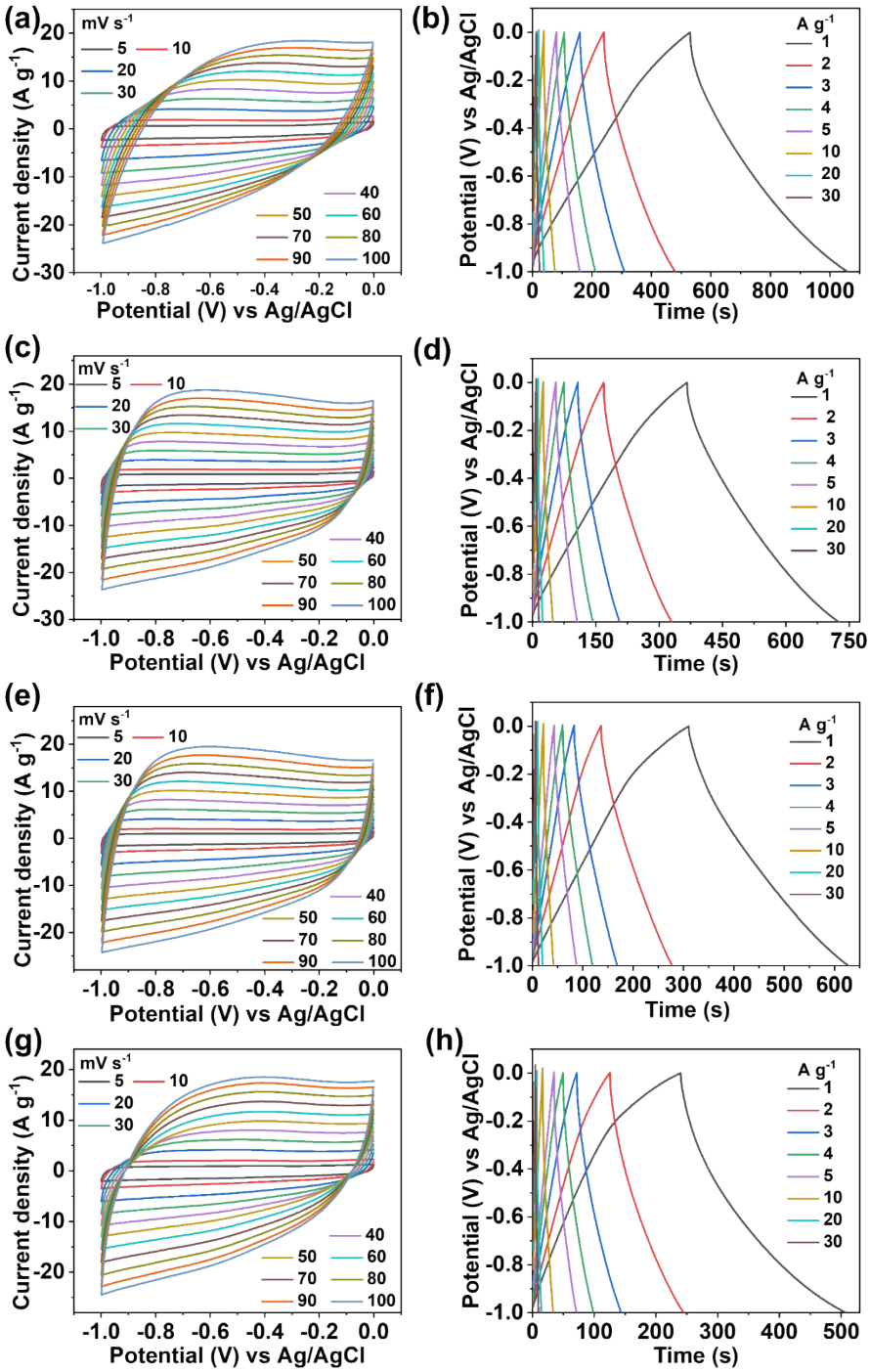

Fig. S18. Electrochemical performances (CV & GCD curves) of (a,b) MX-10@PCNF, (c,d) MX-2@PCNF, (e,f) MX-1@PCNF, and (g,h) PCNF.

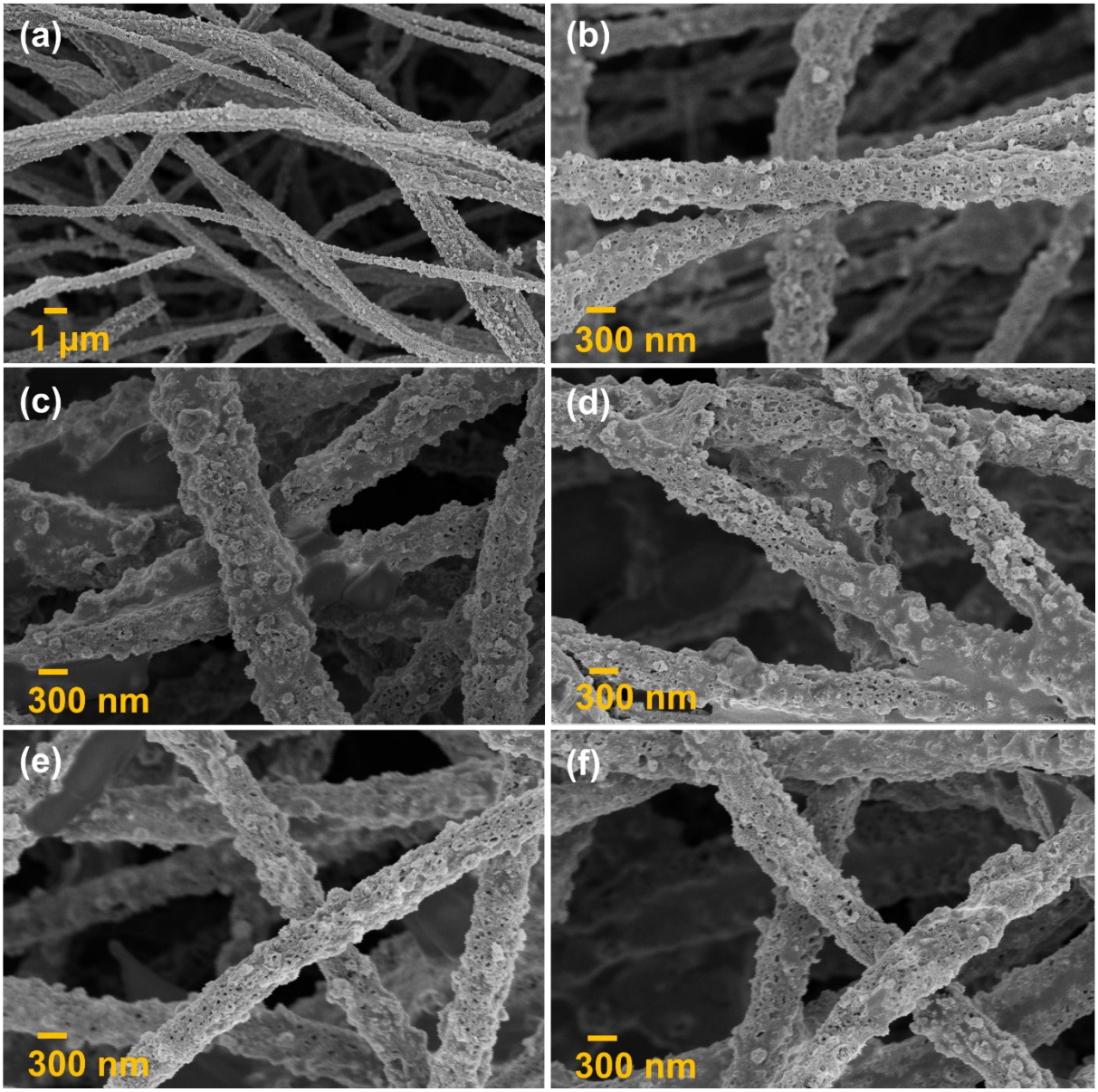

Fig. S19. FESEM images after the stability test, (a-b) MX-5@PCNF at different magnifications, (c) MX-10@PCNF, (d) MX-2@PCNF, (e) MX-1@PCNF, and (f) PCNF.

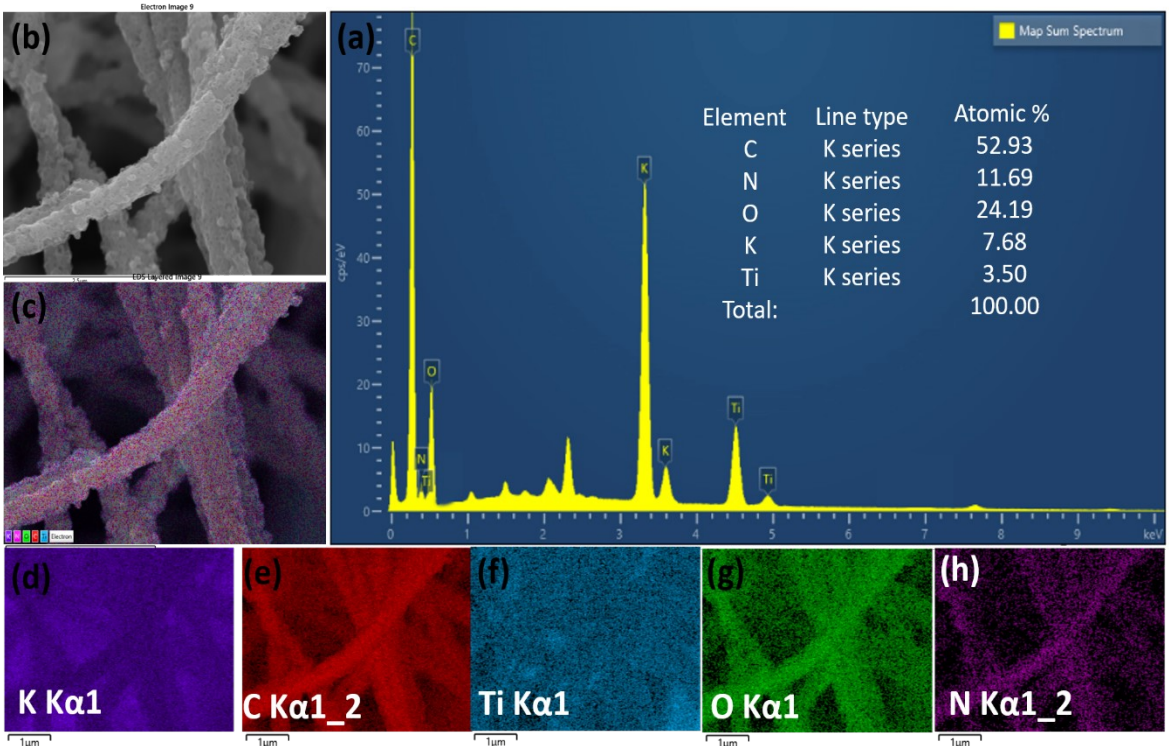

Fig. S20. EDX analysis of MX-5@PCNF after electrochemical test, (a) EDX spectrum (inset: atomic percentage of the different elements), (b-c) sum elemental spectrum, and elemental mapping spectra of (d) K, (e) C, (f) Ti, (g) O, and (h) N.

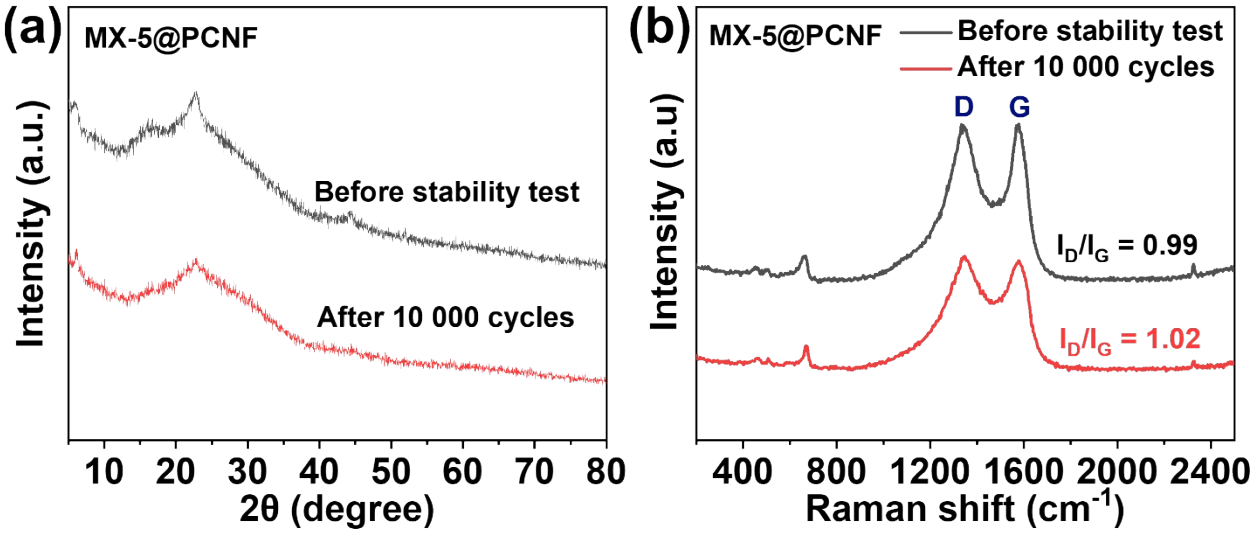

Fig. S21. (a) XRD patterns before and after stability test, and (b) Raman spectra before and after stability test.

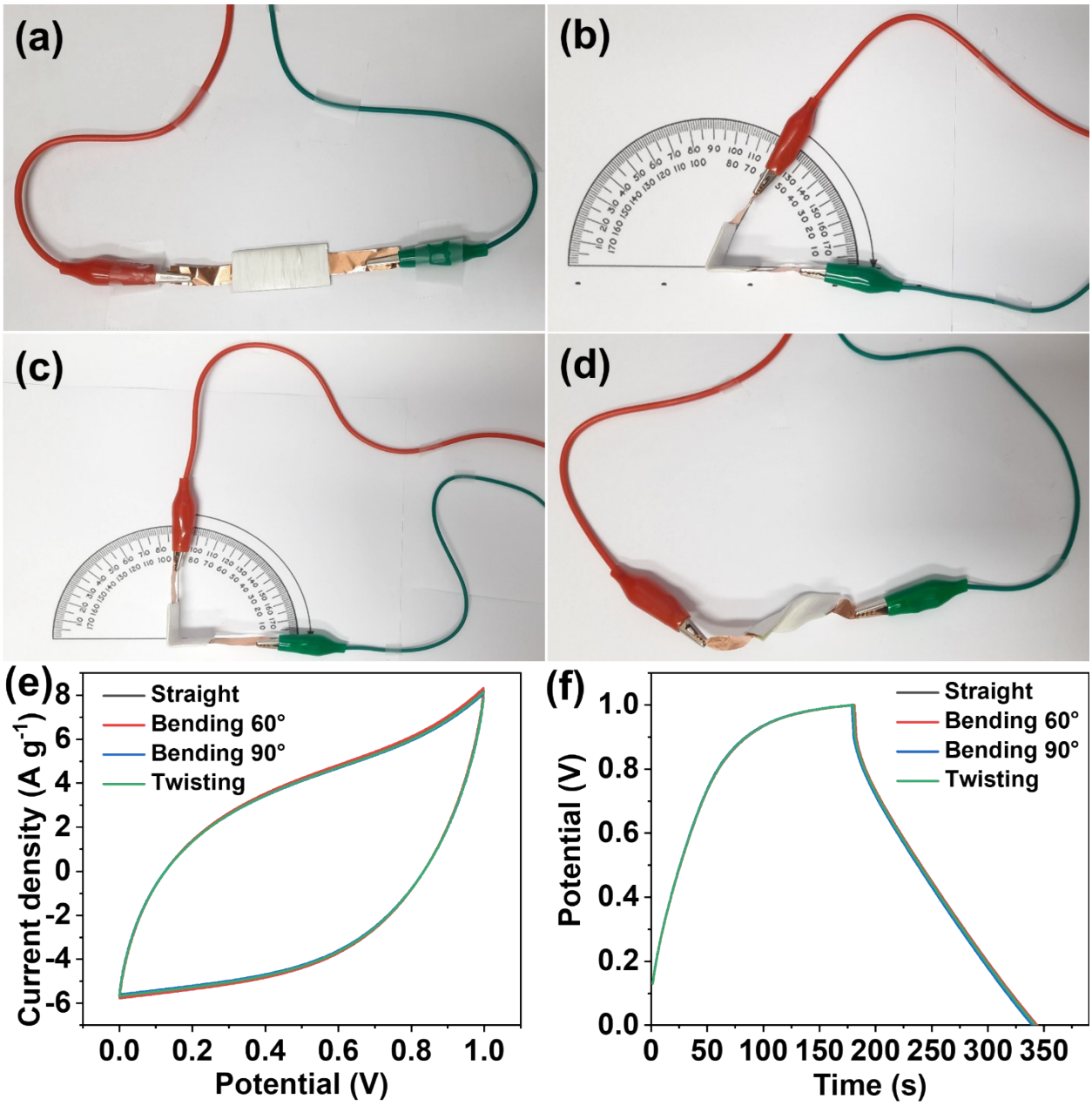

Fig. S22. Digital images of SSC device tested under different conditions (a) straight, (b) bending 60°, (c) bending 90°, and (d) twisting. (e) CV curves (at 50 mV s^{-1}) of the SSC device at straight, bending (at 60° and 90°), and twisting conditions, and (f) GCD curves (at 1 A g^{-1}) of the SSC device at straight, bending (at 60° and 90°), and twisting conditions.

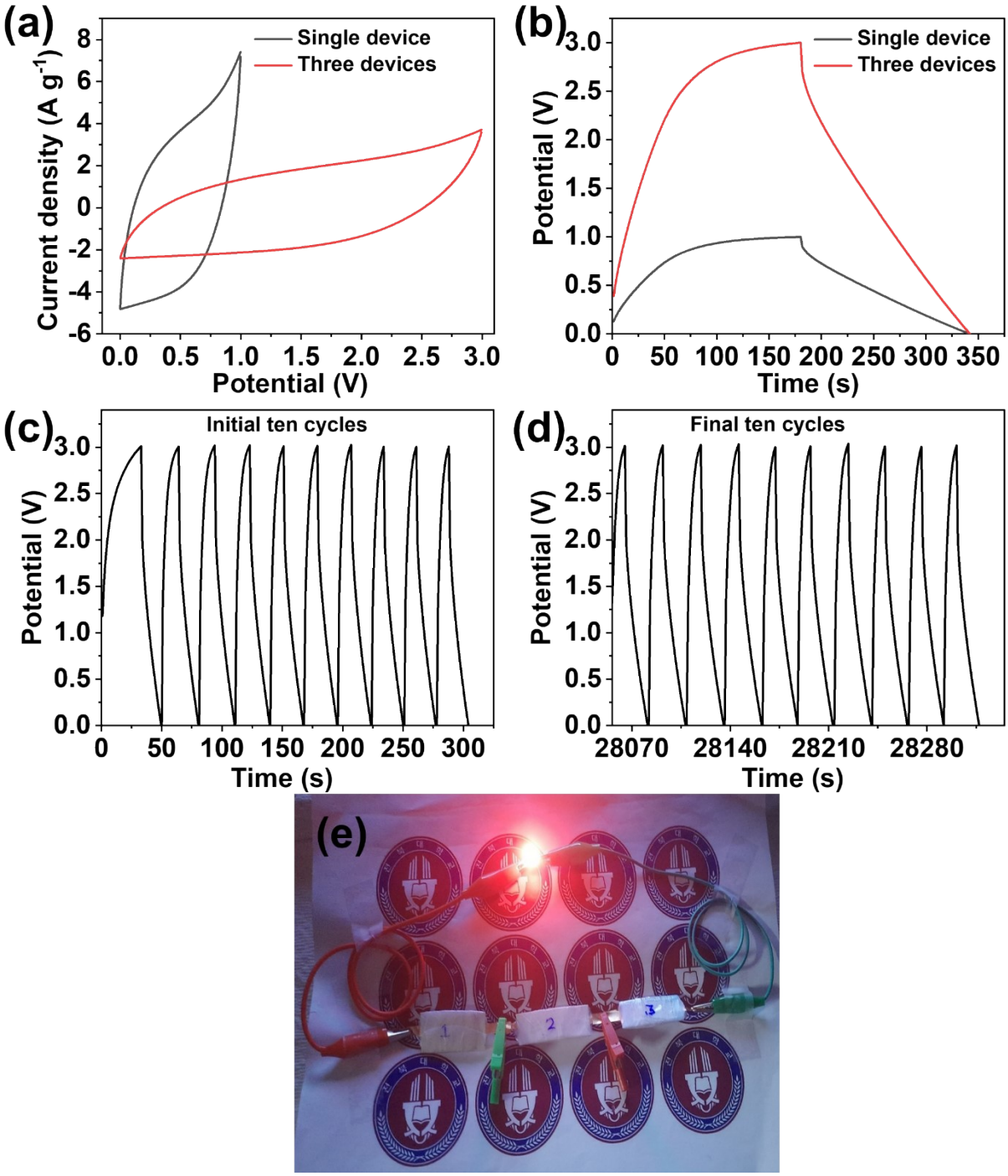

Fig. S23. Electrochemical performance of single SSC device and three SSC devices connected in series (a) CV curves at 50 mV s^{-1}, and (b) GCD curves at 1 A g^{-1}. (c) Initial ten GCD curves of three SSC devices connected in series (at 5 A g^{-1}) at the working potential of 0 to 3.0 V during 1000 GCD cycles and (d) last ten cycles, and (e) digital image of a 1 W red LED powered by three flexible SSC devices connected in series after 1000 GCD cycles at 5 A g^{-1}.

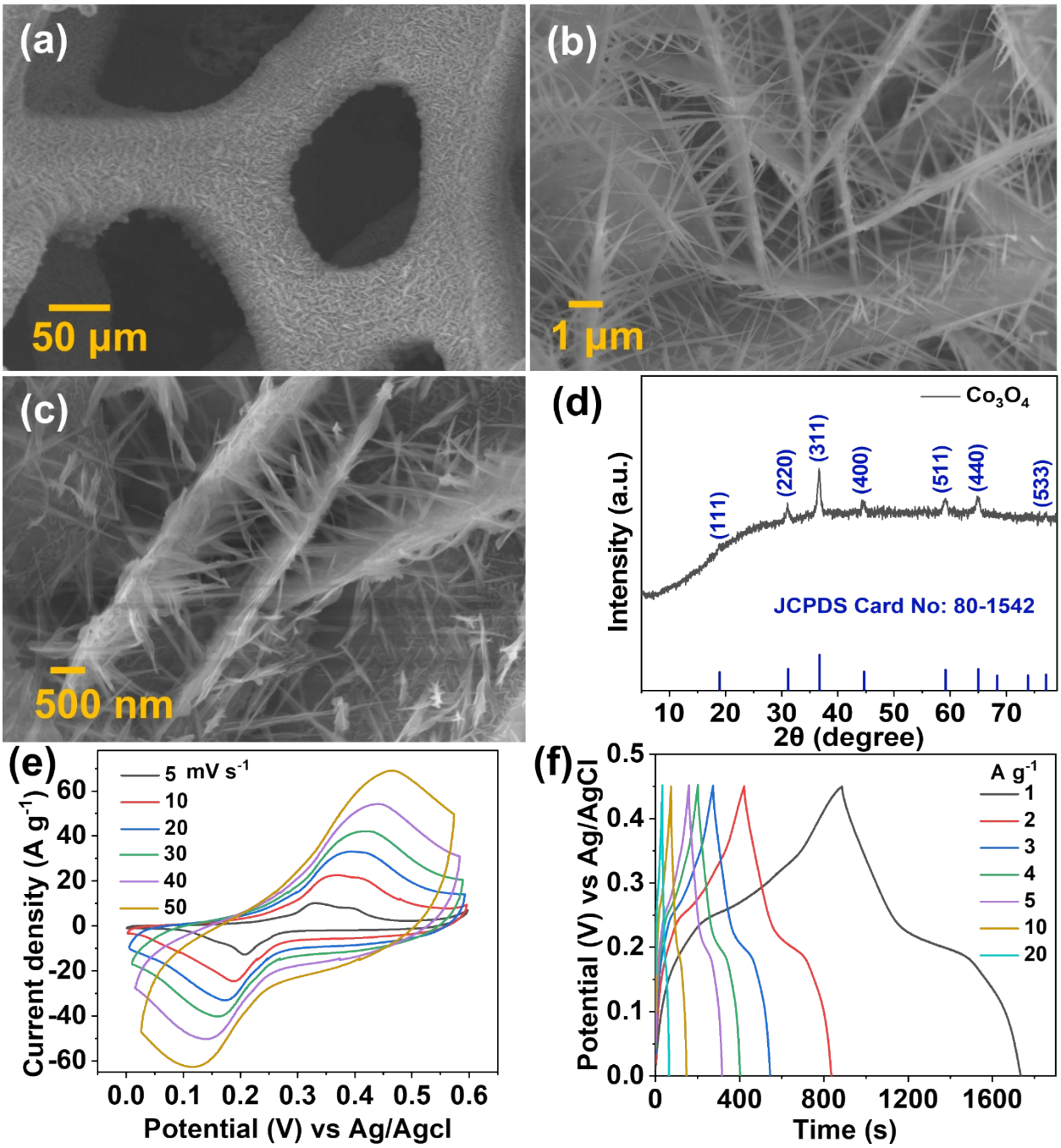

Fig. S24. (a-c) FESEM images of Co_3O_4@NF at different magnifications, (d) XRD patterns of Co_3O_4 powder, and electrochemical performance of the Co_3O_4@NF positive electrode (e) CV curves, and (f) GCD curves. Co_3O_4@NF delivered a capacitance of 1891 F g^{-1} at 1 A g^{-1}.

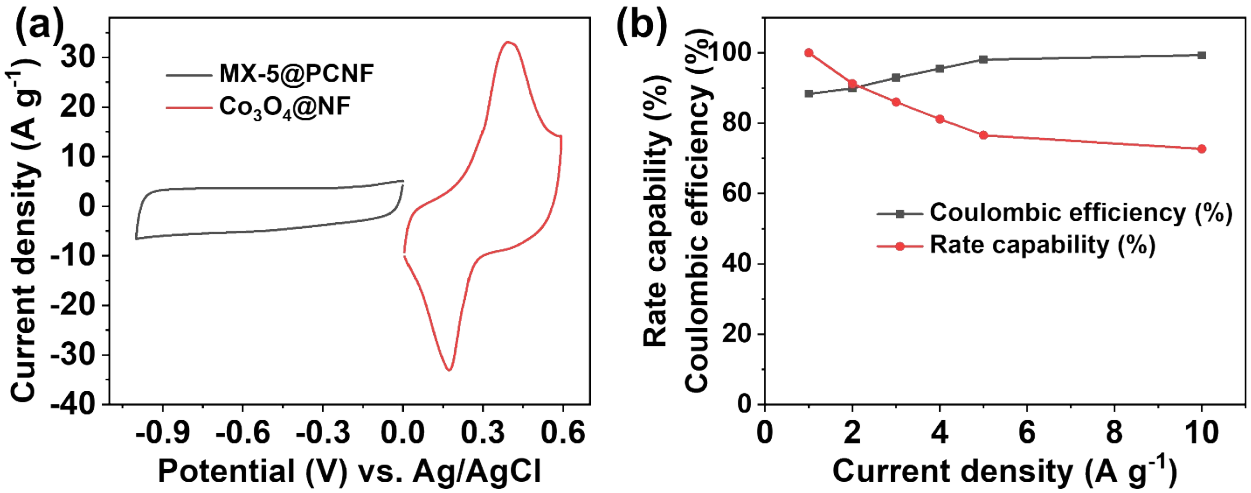

Fig. S25. (a) Comparative CV curves of the negative and positive electrodes (at 20 mV s^{-1}) showing the extension of the working potential of the ASC device up to 1.6 V, and (b) plot showing rate capability and coulombic efficiency at different current densities for Co_3O_4@NF//MX-5@PCNF ASC device.

Table S1. Atomic % of different elements present in MXene from XPS and EDX analysis

Element	**Atomic % (from XPS analysis)**	**Atomic % (from EDX analysis)**
Ti	25.84	25.56
F	30.19	30.81
C	27.41	28.40
O	15.60	15.16
Al	0.04	0.07

Table S2. Elemental compositions of different elements present in different fibers from EDX analysis

Sample	**Weight % of**					
	Carbon (C)	**Nitrogen (N)**	**Cobalt (Co)**	**Oxygen (O)**	**Titanium (Ti)**	**Fluorine (F)**
MX-1/$Co(NO_3)_2$@ PAN	58.07	25.84	7.36	7.27	1.00	0.45
MX-2/$Co(NO_3)_2$@ PAN	58.78	23.11	7.56	7.02	2.82	0.70
MX-5/$Co(NO_3)_2$@ PAN	**56.59**	**22.99**	**7.03**	**7.33**	**4.86**	**1.20**
MX-10/$Co(NO_3)_2$@ PAN	52.33	21.03	7.24	7.55	10.56	1.29

Table S3. BET texture properties of different samples.

Sample	**BET surface area, S_{BET} [$m^2 g^{-1}$]**	**Total pore volume, V_T [$cm^3 g^{-1}$]**	**Average pore diameter, R_{av} [nm]**
PCNF	267.69	0.489	11.71
MX-1@PCNF	291.06	0.504	8.23
MX-2@PCNF	310.54	0.545	7.41
MX-5@PCNF	**405.59**	**0.737**	**4.88**
MX-10@PCNF	385.45	0.676	5.98

Table S4. Nyquist impedance parameters of the different electrodes (PCNF, MX-1@PCNF, MX-2@PCNF, MX-5@PCNF, and MX-10@PCNF).

Sample	**R_s [Ω]**	**R_{ct} [Ω]**	**R_w [Ω]**
PCNF	0.94	1.58	0.06
MX-1@PCNF	0.93	1.52	0.06
MX-2@PCNF	0.93	0.97	0.05
MX-5@PCNF	**0.92**	**0.71**	**0.04**
MX-10@PCNF	0.93	1.51	0.05

Table S5. Nyquist impedance parameters of the SSC device.

Device MX-5@PCNF//MX-5@PCNF	**R_s [Ω]**	**R_{ct} [Ω]**	**R_w [Ω]**	**ESR [Ω]**
Before stability	0.91	0.9	0.04	1.85
After stability	1.11	0.91	0.05	2.07

Table S6. Nyquist impedance parameters of the ASC device.

Device Co_3O_4@NF//MX-5@PCNF	**R_s [Ω]**	**R_{ct} [Ω]**	**R_w [Ω]**	**ESR [Ω]**
Before stability	0.71	4.98	0.04	5.73
After stability	0.84	6.93	0.05	7.82

Table S7. Comparison of the electrochemical performances of MX-5@PCNF with similar electrode materials.

Electrode materials	**Electrolyte**	**Potential window [V]**	**Specific capacitance, C_s [F g^{-1}]**	**Current density [A g^{-1}]**	**Cyclic stability**	**Ref.**
Co-PC@MX-CNF	2 M KOH	-1 to 0	426.7	1	95.12% after 10000 cycles	[3]
$Ti_3C_2T_x$ MXene	1 M H_2SO_4	-0.3 to -0.35	213.5	1	-	[4]
$Ti_3C_2T_x$ MXene	6 M KOH	-0.8 to 0	283	1	84% after 10000 cycles	[5]
N-CNTs/MXene /PAN	1 M H_2SO_4	-0.6 to 0.1	446.12	5 (mV s^{-1})	90.9% after 10000 cycles	[6]
$Ti_3C_2T_x$ / MoO_3	1 M Na_2SO_4	-1 to 0.1	371 C g^{-1}	1	89.5% after 6000 cycles	[7]
MXene/CFT	1 M KOH	-1 to 0	474.23	1.5	97.52% after 10000 cycles	[8]
$Ti_3C_2T_x$ / CC	1 M LiCl	-0.7 to 0	155	1	-	[9]
$Ti_3C_2T_x$ / α-Fe_2O_3	5 M LiCl	-1.2 to 0	405.4	2	97.7% after 2000 cycles	[10]
$Ti_3C_2T_x$ / PANI	1 M H_2SO_4	-0.7 to 0.2	652.3	1	99% after 10000 cycles	[11]
MXene-Polyindole (3:1)	1 M KOH & 1 M KCl	-1.3 to 0	226.5	2	90.5% after 8000 cycles	[12]
CC/MXene	1 M H_2SO_4	-0.3 to 0.3	240.7	1	-	[13]
$Ti_3C_2T_x$/Bi_2S_3@N-C	1 M KOH	-1 to 0	653	1	-	[14]
d-Ti_3C_2 film	6 M KOH	-1.2 to -0.1	153.9 C g^{-1}	1	100% after 10000 cycles	[15]
CQDs@$Ti_3C_2T_x$	1 M H_2SO_4	-0.55 to 0.3	441.3	1	100% after 10000 cycles	[16]
Na-$Ti_3C_2T_x$	1 M H_2SO_4	-0.4 to 0.2	578	1	92% after 10000 cycles	[17]
MX-5@PCNF	**3 M KOH**	**-1.0 to 0**	**572.7**	**1**	**96.4% after 10000 cycles**	**This work**

Table S8. Comparison of the energy density and power density of the MX-5@PCNF//MX-5@PCNF symmetric device with similar symmetric devices.

Device (symmetric)	**Electrolyte**	**Potential window [V]**	**Energy density [Wh kg^{-1}]**	**Power density [W kg^{-1}]**	**Cyclic stability**	**Ref.**
A-$Ti_3C_2T_x$/PANI	1 M H_2SO_4	1.0	20.3	500	-	[11]
$RuCo_2O_4$/$Ti_3C_2T_x$@NF	1M KOH	0.8	20.4	2400	90% after 5000 cycles	[18]
Bi_2S_3/$Ti_3C_2T_x$	1 M KOH	1.3	27.6	24300	91% after 5000 cycles	[19]
N, O co-doped C@Ti_3C_2	6 M KOH	1.2	10.8	600	90% after 5000 cycles	[20]
ZIF67/rGO composite	0.2 M $K_3[Fe(CN)_6]$ in 1 M Na_2SO_4	1.5	25.5	2700	88% after 1000 cycles	[21]
MXene/PANI	PVA/H_2SO_4	1.2	31.18	1079.3	71.4% after 4000 cycles	[22]
$Ti_3C_2T_x$/rGO-4	1 M H_2SO_4	1.0	7.5	500	80% after 4000 cycles	[23]
$Ti_3C_2T_x$ rGO	PVA-H_2SO_4	0.7	9.38	346800	-	[24]
$Ti_3C_2T_x$@PEDOT	1 M H_2SO_4	1.6	6.34	4077000	-	[25]
3D $Ti_3C_2T_x$ /CNTs	3 M H_2SO_4	1.0	23.9	498.6	95.9% after 10000 cycles	[26]
S, N co-doped rGO/MXene	PVA-KOH	1.4	24.2	1400.6	-	[27]
MXene-NCF (N-doped carbon foam)	PVA-KOH	1.0	8.75	1871	99.2% after 10000 cycles	[28]
MXene-PANI/α-Fe_2O_3-MnO_2	PVA-H_2SO_4 hydrogel	0.8	17.45	1056.87	91.2% after 10000 cycles	[29]
MoS_2-$Ti_3C_2T_x$	1 M H_2SO_4	0.6	5.1	298	72.3% after 10000 cycles	[30]
WSe_2/MXene	6 M KOH	0.6	12.3	600	97% after 5000 cycles	[31]
MXene/FMP/MXene	PVA-H_2SO_4	0.8	12.38	760.32	90.4% after 5000 cycles	[32]
V_2CT_x/ $Ti_3C_2T_x$	1 M H_2SO_4	0.7	5.4	357.8	94.5% after	[33]

					10000 cycles	
C67@PAN-OC	Gel electrolyte	0.8	9.6	550	59.5% after 1000 cycles	[34]
MX-5@PCNF	**3 M KOH**	**1.0**	**22.53**	**499.99**	**91.3% after 10000 cycles**	**This work**

Table S9. Comparison of the energy density and power density of the Co_3O_4@NF//MX-5@PCNF asymmetric device with similar asymmetric devices.

Device (asymmetric)	**Electrolyte**	**Potential window [V]**	**Energy density [Wh kg^{-1}]**	**Power density [W kg^{-1}]**	**Cyclic stability**	**Ref.**
ZCO//MXene	KOH hydrogel	1.6	99.94	800	>94% after 5000 cycles	[8]
MnO_2//MXene-Polyindole (3:1)	1M $TEABF_4$/ DMSO	1.8	65.3	2000	93.58% after 6000 cycles	[12]
Mxene/$CuCo_2S_4$//AC	6 M KOH	1.6	66.8	895.1	88.2% after 10000 cycles	[35]
MXene-NPO//rGO	KOH/PVA	1.5	72.6	932	94% after 10000 cycles	[36]
HS-NCS@MXene//AC-AHSC	2 M KOH	1.6	80.0	1196	92% after 10000 cycles	[37]
NiCo-MOF/Ti_3C_2Tx//AC	2 M KOH	1.5	39.5	562.5	82.3% after 10000	[38]
MXene/$NiCo_2S_4$@CC//NACC	6 M KOH	1.6	57.5	800	90.2% after 5000 cycles	[39]
MnO_2@Co_3O_4-PC@MX-CNF// PC@MX-CNF	PVA/KOH	1.6	72.5	832.4	90.36% after 10000 cycles	[3]
B-GC@CPP-4//MXene	PVA/KOH	1.6	45	1735	96% after 10000 cycles	[40]
rGO/PANI//P-MXene/C_{PAQ}-A	3 M H_2SO_4	1.5	38.7	497.7	-	[41]
CNT-HQ//$Ti_3C_2T_x$ MXene	PVA/H_2SO_4	1.6	62	281	Nearly 100% after 5000 cycles	[42]
M/CoS_2/CCS-5// MXene-Polyindole	1 M $TEABF_4$ in DMSO	1.6	42.2	1801.5	96% after 10000 cycles	[43]
rGO/MXene@$NiCoO_2$//	PVA-KOH	1.6	45.15	394.52	82.69% after	[44]

rGO/MXene					10000 cycles	
$Co_3O_4/Ti_3C_2T_x$//AC	PVA/KOH	1.4	95.9	630.4	80.0% after 10000 cycles	[45]
$NiCo_2Se_4$/MXene//AC	3 M KOH	1.6	22.4	800	60.8% after 10000 cycles	[46]
CF-$NiCo_2S_4$//MXene	0.5 M K_2SO_4	1.2	14.86	8197	85% after 10000 cycles	[47]
$Cu_{0.5}Co_{0.5}Se_2$//$Ti_3C_2T_x$ MXene	PVA-KOH	1.6	84.17	604	91.1% after 10000 cycles	[48]
Co_3O_4@NF//MX-5@PCNF	**3 M KOH**	**1.6**	**74.2**	**800**	**87.78% after 10000 cycles**	**This work**

References:

1. T. Mukhiya, B. Dahal, G. P. Ojha, K. Chhetri, M. Lee, T. Kim, S.-H. Chae, A. P. Tiwari, A. Muthurasu and H. Y. Kim, *Compos. B Eng.*, 2019, **178**, 107482.
2. T. Mukhiya, G. P. Ojha, B. Dahal, T. Kim, K. Chhetri, M. Lee, S.-H. Chae, A. Muthurasu, A. P. Tiwari and H. Y. Kim, *ACS Appl. Energy Mater.*, 2020, **3**, 3435-3444.
3. T. Kshetri, D. D. Khumujam, T. I. Singh, Y. S. Lee, N. H. Kim and J. H. Lee, *Chem. Eng. J.*, 2022, **437**, 135338.
4. X. Chu, Y. Wang, L. Cai, H. Huang, Z. Xu, Y. Xie, C. Yan, Q. Wang, H. Zhang, H. Li and W. Yang, *SusMat*, 2022, **2**, 379-390.
5. S. Venkateshalu and A. N. Grace, *Electrochim. Acta*, 2020, **341**, 136035.
6. D.-D. Li, Q. Yuan, L.-Z. Huang, W. Zhang, W.-Y. Guo and M.-G. Ma, *Ind. Eng. Chem. Res.*, 2021, **60**, 15352-15363.
7. Z. Pan, C. Yang, Y. Li, X. Hu and X. Ji, *Chem. Eng. J.*, 2022, **428**, 131138.
8. M. S. Javed, H. Lei, H. U. Shah, S. Asim, R. Raza and W. Mai, *J. Mater. Chem. A*, 2019, **7**, 24543-24556.
9. X. Chen, F. Su, Q. Zhou and J. Sun, *Surf. Interfaces*, 2021, **26**, 101393.
10. R. Zou, H. Quan, M. Pan, S. Zhou, D. Chen and X. Luo, *Electrochim. Acta*, 2018, **292**, 31-38.
11. W. Liu, Y. Zheng, Z. Zhang, Y. Zhang, Y. Wu, H. Gao, J. Su and Y. Gao, *J. Power Sources*, 2022, **521**, 230965.

12. S. De, C. K. Maity, S. Sahoo and G. C. Nayak, *ACS Appl. Energy Mater.*, 2021, **4**, 3712-3723.
13. Y. Wei, W. Luo, X. Li, Z. Lin, C. Hou, M. Ma, J. Ding, T. Li and Y. Ma, *Electrochim. Acta*, 2022, **406**, 139874.
14. W. Zhang, H. Jiang, Y. Li, W. Ma, X. Yang and J. Zhang, *J. Alloys Compd.*, 2021, **883**, 160881.
15. Y. Luo, C. Yang, Y. Tian, Y. Tang, X. Yin and W. Que, *J. Power Sources*, 2020, **450**, 227694.
16. Y. Wang, Y. Cui, D. Kong, X. Wang, B. Li, T. Cai, X. Li, J. Xu, Y. Li, Y. Yan, H. Hu, M. Wu, Q. Xue, Z. Yan, L. Zhao and W. Xing, *Carbon*, 2021, **180**, 118-126.
17. X. Hu, Q. Zhang, N. Gong, X. Chen, L. Wang, W. Peng, Y. Li, F. Zhang and X. Fan, *Energy Storage Mater.*, 2022, **50**, 802-809.
18. P. Asen, A. Esfandiar and H. Mehdipour, *Nanoscale*, 2022, **14**, 1347-1362.
19. Y. Li, Y. Deng, X. Zhang, G. Ying, Z. Wang and J. Zhang, *Electrochim. Acta*, 2021, **366**, 137406.
20. Z. Pan and X. Ji, *J. Power Sources*, 2019, **439**, 227068.
21. S. Sundriyal, V. Shrivastav, H. Kaur, S. Mishra and A. Deep, *ACS Omega*, 2018, **3**, 17348-17358.
22. W. Luo, Y. Wei, Z. Zhuang, Z. Lin, X. Li, C. Hou, T. Li and Y. Ma, *Electrochim. Acta*, 2022, **406**, 139871.
23. B. Guo, J. Tian, X. Yin, G. Xi, W. Wang, X. Shi and W. Wu, *Colloids Surf. A: Physicochem. Eng. Asp.*, 2020, **595**, 124683.
24. J. Zhang, D. Jiang, L. Liao, L. Cui, R. Zheng and J. Liu, *Chem. Eng. J.*, 2022, **429**, 132232.
25. Z. Liu, L. Wang, Y. Xu, J. Guo, S. Zhang and Y. Lu, *J. Electroanal. Chem.*, 2021, **881**, 114958.
26. P. Zhang, Q. Zhu, R. A. Soomro, S. He, N. Sun, N. Qiao and B. Xu, *Adv. Funct. Mater.*, 2020, **30**, 2000922.
27. X. Liu, Z. Lu, X. Huang, J. Bai, C. Li, C. Tu and X. Chen, *J. Power Sources*, 2021, **516**, 230682.

28. L. Sun, G. Song, Y. Sun, Q. Fu and C. Pan, *ACS Appl. Mater. Interfaces*, 2020, **12**, 44777-44788.
29. C. Li, S. Wang, Y. Cui, X. Wang, Z. Yong, D. Liang, Y. Chi and Z. Wang, *J. Colloid Interface Sci.*, 2022, **620**, 35-46.
30. W. Hou, Y. Sun, Y. Zhang, T. Wang, L. Wu, Y. Du and W. Zhong, *J. Alloys Compd.*, 2021, **859**, 157797.
31. S. Hussain, D. Vikraman, M. T. Mehran, M. Hussain, G. Nazir, S. A. Patil, H.-S. Kim and J. Jung, *Renew. Energy*, 2022, **185**, 585-597.
32. C. Li, S. Wang, Y. Cui, X. Wang, Z. Yong, D. Liang, Y. Chi and Z. Wang, *ACS Appl. Mater. Interfaces*, 2022, **14**, 9172-9182.
33. K. Chen, Y. Guan, Y. Cong, H. Zhu, K. Li, J. Wu, Z. Dong, G. Yuan, Q. Zhang and X. Li, *J. Alloys Compd.*, 2022, **906**, 164302.
34. C.-H. Yang, Y.-C. Hsiao and L.-Y. Lin, *ACS Appl. Mater. Interfaces*, 2021, **13**, 41637-41648.
35. X. Chen, Z. Ding, H. Yu, H. Ge, W. Liu and S. Sun, *Mater. Chem. Front.*, 2021, **5**, 7606-7616.
36. H. Zhang, Z. Li, Z. Hou, H. Mei, Y. Feng, B. Xu and D. Sun, *Chem. Eng. J.*, 2021, **425**, 130602.
37. M. S. Javed, X. Zhang, S. Ali, A. Mateen, M. Idrees, M. Sajjad, S. Batool, A. Ahmad, M. Imran, T. Najam and W. Han, *Nano Energy*, 2022, **101**, 107624.
38. Y. Wang, Y. Liu, C. Wang, H. Liu, J. Zhang, J. Lin, J. Fan, T. Ding, J. E. Ryu and Z. Guo, *Eng. Sci.*, 2020, **9**, 50-59.
39. L. Li, J. Fu, Y.-R. Cho, J. M. Yun, Y. S. Jung, S. H. Kwon and K. H. Kim, *Appl. Surf. Sci.*, 2021, **549**, 149226.
40. A. Padhy, R. Samal, C. S. Rout and J. N. Behera, *Sustain. Energy Fuels*, 2022, **6**, 2010-2019.
41. R. Ma, X. Zhang, J. Zhuo, L. Cao, Y. Song, Y. Yin, X. Wang, G. Yang and F. Yi, *ACS Nano*, 2022, **16**, 9713-9727.
42. M. Hu, T. Hu, Z. Li, Y. Yang, R. Cheng, J. Yang, C. Cui and X. Wang, *ACS Nano*, 2018, **12**, 3578-3586.

43. S. De, C. K. Maity, S. Acharya, S. Sahoo, J.-J. Shim and G. C. Nayak, *J. Energy Storage*, 2022, **50**, 104617.
44. C. Li, G. Jiang, T. Liu, Z. Zeng, P. Li, R. Wang and X. Zhang, *J. Energy Storage*, 2022, **49**, 104176.
45. S. Li, J. Fan, G. Xiao, S. Gao, K. Cui and Z. Chao, *Int. J. Hydrog. Energy*, 2022, **47**, 22663-22679.
46. Y. Liu, J. Gong, J. Wang, C. Hu, M. Xie, X. Jin, S. Wang and Y. Dai, *J. Alloys Compd.*, 2022, **899**, 163354.
47. M. Pathak, S. R. Polaki and C. S. Rout, *RSC Adv.*, 2022, **12**, 10788-10799.
48. Y. Abu Dakka, J. Balamurugan, R. Balaji, N. H. Kim and J. H. Lee, *Chem. Eng. J.*, 2020, **385**, 123455.